Widespread subseafloor gas hydrate in the Barents Sea and Norwegian Margin

A.E. Cook[1*], A. Portnov[2], R.C. Heber[1], S. Vadakkepuliyambatta[3,4] and S. Bünz[3]

[1]Ohio State University, Columbus, Ohio, USA

[2]Univeristy of Texas at Austin, Austin, Texas, USA

[3]CAGE-Centre for Arctic Gas Hydrate, Environment and Climate, UiT-The Arctic University of Norway, Tromsø, Norway

[4]National Centre for Polar and Ocean Research (NCPOR), Ministry of Earth Sciences, Government of India, Goa, India

*Corresponding Author: cook.1129@osu.edu

Abstract

The distribution and concentration of subseafloor natural gas hydrate across margins is not well understood, because these systems are challenging to image and quantify remotely. Furthermore, it is unknown if shallow hydrate systems are linked to deeper oil and gas reservoirs. Herein, we analyze petroleum industry well logs with data in the gas hydrate stability zone and find that low concentrations of hydrate commonly occur below the seafloor in the Barents Sea and the Norwegian Margin. We observe hydrate in half of analyzed industry wells using a set of conservative criteria that requires a resistivity increase of at least 0.5 Ωm above background resistivity. Hydrate accumulations occur significantly above the base of the hydrate stability zone, in layers with thicknesses ranging from tens of centimeters to tens of meters. Moreover, we find that there is no relationship between wells with hydrate accumulations and deeper oil and gas reservoirs; hydrate is just as likely to occur above identified oil and gas reservoirs as in areas with dry holes (i.e., no oil or gas reservoir). We argue the low concentration of hydrate, the occurrence of hydrate significantly above the base of the gas hydrate stability zone, and the lack of association between hydrate occurrence and deeper oil and gas reservoirs implies that the gas in these hydrate systems is likely transported via diffusion and is primarily microbial in origin.

1. Introduction

Natural gas hydrate is a significant methane reservoir, estimated to store ~5-20% of Earth's mobile carbon (Boswell and Collett, 2011; Ruppel and Kessler, 2017). Most natural gas hydrate on Earth occurs within marine sediments on continental slopes, yet how natural gas hydrate distributes and concentrates within hydrate systems and across basins and margins is largely unknown. As the Earth warms, gas hydrate systems near the landward limit of hydrate stability or in Arctic regions are more vulnerable to dissociation (Archer, 2007; Gorman and Senger, 2010; Phrampus and Hornbach, 2012). Therefore, the location, concentration and distribution of hydrate will directly influence the flow of carbon to the ocean and atmosphere. In addition, when hydrate dissociates, it can increase pore pressure which may lead to slope instability, reduced shear strength and submarine landslides (Maslin et al., 2010).

Reflection seismic surveys, the most widely used geophysical technique for identifying hydrate systems, rarely detects gas hydrate itself. Seismic data can only detect thick (at least 6-12 m, depending on signal frequency) high saturation layers of gas hydrate; this is due to the resolution of seismic data and the fact that hydrate saturations less than ~40% do not strongly affect compressional velocity (Yun et al., 2005). Instead, seismic data is usually used to identify bottom simulating reflections (BSRs), which are a negative acoustic impedance interface that is caused by free gas at the base of gas hydrate stability (Haacke et al., 2007; Shipley et al., 1979). The BSR usually approximates the thermodynamic interface that separates gas hydrate above from free gas below. The presence of a BSR, however, provides little to no information about the concentration and distribution of gas hydrate within the gas hydrate stability zone (GHSZ), meaning the characteristics of most gas hydrate systems are broadly unknown.

Unlike lower-resolution seismic data, a suite of downhole well logs can identify the presence of gas hydrate in specific depth intervals due to their significantly higher vertical resolution. In addition, the wide range of well log measurements potentially provide information about the sediment or rock type, in situ characteristics of hydrate, and hydrate saturation (Goldberg et al., 2010; Tsuji et al., 2009). The most important well log needed to detect hydrate is resistivity; hydrate is an electrical insulator and even small amounts of gas hydrate in the pore space or in a fracture increases the measured resistivity.

Well logs along with sediment cores and pressure cores are often collected as a part of scientific ocean drilling programs and state-funded hydrate drilling programs in China, India, Japan, South Korea and the United States (Barnes et al., 2019; Collett et al., 2019; Flemings et al., 2020; Tamaki et al., 2017). While these drilling campaigns provide valuable information and excellent datasets, they usually focus on the rare areas where high-saturation hydrate is detectable on seismic data or in the environments that are favorable to high-saturation hydrate.

This leaves us with very little information on lower saturation gas hydrate systems that very likely constitute the overwhelming majority of hydrate systems on Earth.

Herein, we use industry well log and drilling data archived by the Norwegian Petroleum Directorate in the Barents Sea and on the mid Norwegian Margin to illuminate gas hydrate occurrence and distribution below the seafloor, similar to the approach used in the Gulf of Mexico by Majumdar et al. (2017). The industry wells used herein always have resistivity and gamma ray well logs in the GHSZ, and some industry wells also have additional data making the analysis more robust. Importantly, industry wells are usually drilled in areas that have no evidence of fluid flow or shallow gas, meaning that the well log data is collected in systems that are more likely to represent baseline or background gas hydrate systems.

2. Geologic Setting & Hydrate Occurrence

This study is focused on the sub-Arctic Norwegian Margin and the Arctic Barents Sea, both coastal waters of Norway.

2.1 Barents Sea

The Barents Sea lies at the intersection of warm Atlantic waters and cold Arctic waters, making it an Arctic climate transition zone (Loeng, 1991). Over the Cenozoic, the area has been shaped by a complex geologic history involving tectonic uplift, subsidence and glacial erosion (Faleide et al., 1984; Lasabuda et al., 2021; Vorren et al., 1991). These geologic processes likely promoted subseafloor fluid flow and gas seepage into the water column, resulting in extensive pockmark fields and craters on the modern seafloor (Andreassen et al., 2017; Nixon et al., 2019; Rise et al., 2014; Serov et al., 2017; Solheim and Elverhøi, 1985). Sub-seafloor fluid migration in the Barents Sea is controlled by gas chimneys, faults and fractures, which are potential pathways for natural gas to flow into the GHSZ (Laberg et al., 1998; Ostanin et al., 2013; Vadakkepuliyambatta et al., 2017, 2013).

Compared to many continental slopes that host gas hydrate in more temperate environments, the Barents Sea is quite shallow, with an average water depth of ~230 m. In addition, there is a relatively thin drape of Pliocene to Pleistocene glacial sediments (between 0-1000 m) depending on the location (Vorren et al., 1989). These sediments are underlain by more compact sediments and lithified sedimentary rocks of Paleogene, Cretaceous and Jurassic age (NPD, 2014) .

Gas hydrate could be actively dissociating in the Barents Sea, because global temperature increases have a significant impact on the water temperature in shallow seas (Ferré et al., 2012). Gas hydrate was sampled directly from the seafloor at the Håkon Mosby mud volcano (Pape et al., 2011; Vogt et al., 1997) and farther north at pingo-like features in Storfjordrenna (Serov et al 2017); however, there have been no hydrate samples from subseafloor systems. Therefore, there are many uncertainties regarding hydrate saturation, hydrate distribution, and hydrate volume in the rock and sediment below the seafloor in the Barents Sea (Minshull et al., 2020).

Even so, there is evidence for thermogenic gas hydrate occurring several hundred meters below the seafloor in the Barents Sea. Laberg et al. (1998) observed BSRs in seismic data in the Bear Island Trough at ~220 meters below seafloor (mbsf), where water depths are just over 400 m. For comparison, gas hydrate stability models at water depths 400 m suggest the base of stability is at ~150 mbsf for pure methane systems; the base of stability increases to ~400 mbsf with a gas composition of 96% methane, 3% ethane and 1% propane (Vadakkepuliyambatta et al., 2017). Rajan et al. (2013) similarly observed BSRs at depths ranging from ~225-345 mbsf in Paleogene-Neogene lithified sediments in water depths of 300-350 m. These observations strongly suggest that hydrate accumulations in the Barents Sea have a significant component of higher-order hydrocarbons that increase the depth of the base of the GHSZ relative to pure methane systems (Ostanin et al., 2013; Waage et al., 2019).

2.2 Norwegian Margin

The formation of the Norwegian Margin is a result of multiple rifting events during the Mesozoic that led to the eventual inception of seafloor spreading in the late Cretaceous along the Atlantic mid-ocean ridge (Skogseid and Eldholm, 1995). Thermal subsidence of the crust (Skogseid and Eldholm, 1995), the development of N-S trending domes (Doré and Lundin, 1996) and differential subsidence of sediments on the continental slope (Martinsen et al., 2005) led to the development of a number of sedimentary basins along the margin. These basin are filled with ~10-km-thick deposits of sediment (Brekke, 2000). More recent deposition of sediment on the Norwegian slope is controlled by glacial-interglacial cycles, and that sediment may be redeposited in several different contourite drifts on the continental slope (Laberg et al., 2001).

On the Norwegian Margin, a number of studies focus on gas hydrate near the Storegga Slide, which is one of the largest known submarine landslides having moved 3400 km^3 to 5600 km^3 of sediment during several slope failure events (Bryn et al., 2005; Bugge et al., 1987; Bünz et al., 2003)(Figure 1). Near the headwall and the northern sidewall of the Storegga Slide, BSRs are visible at water depths between 550 to 1300 m (Bünz et al., 2003; Mienert et al., 1998). The modern day BSR is the shallowest along the headwall, at just 185 ms two-way-time, which is ~150 mbsf (Bünz et al., 2003). Hustoft et al.(2007) also observed seafloor pockmarks and fluid migration at the Storegga Slide. Furthermore, hydrate samples were obtained near the seafloor at a pockmark field along the northeastern sidewall of the Storegga Slide (Ivanov et al., 2007). Using velocity data from ocean bottom seismometers, hydrate saturation was estimated from 3-

6% (Bünz et al., 2005) to 10-20% (Westbrook et al., 2008) along the northern sidewall of the Storegga Slide. These estimates have large uncertainties, however, because the physical properties of the sediment and the morphology of the hydrate are not known.

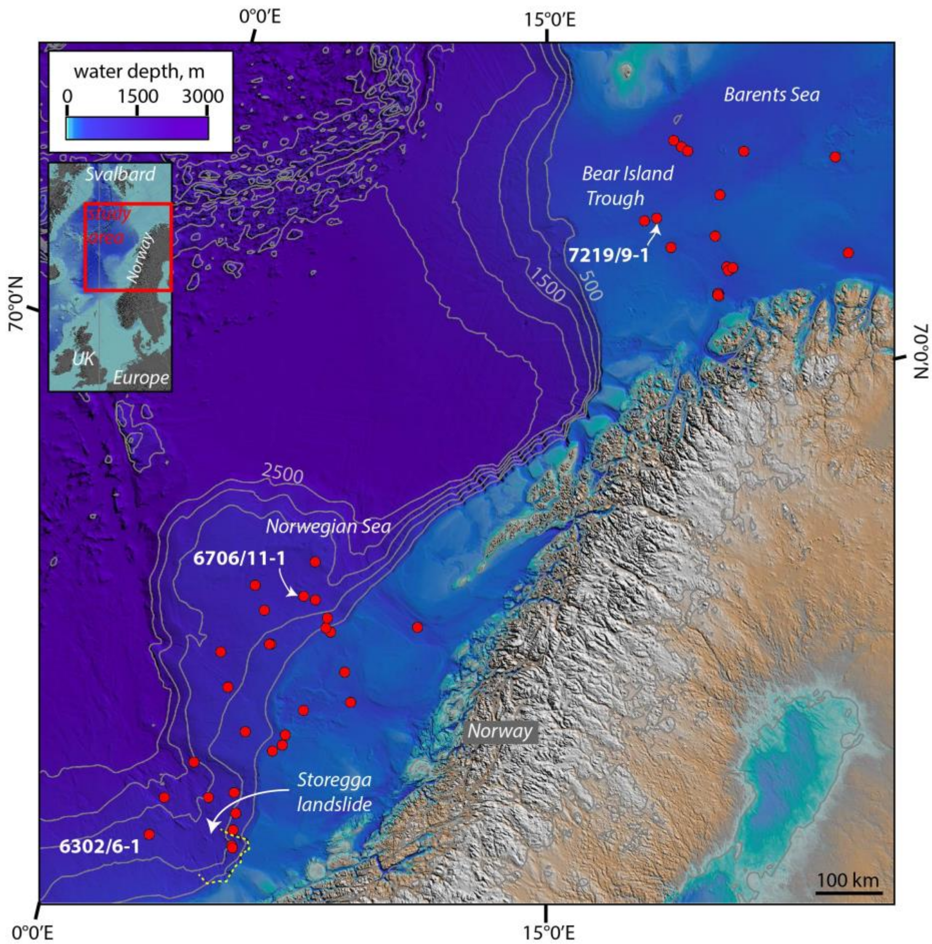

Figure 1. Industry wells (red) with well logging data in the gas hydrate stability zone analyzed herein on the Norwegian Margin and in the Barents Sea.

3. Methods

Well logging data is collected during the drilling and assessment of petroleum industry boreholes. Industry reservoir targets are below the GHSZ, but well logs are often collected through the shallow GHSZ. Publicly available well logs and well data for the Barents Sea and the Norwegian Margin were downloaded from the DISKOS data repository operated by the Norwegian Petroleum Directorate. Well log data was in either a digital file (.las) or an image (jpeg or pdf). The first step in the assessment of the well logs is to determine if any data occurs in the gas hydrate stability zone.

3.1. Gas Hydrate Stability

Hydrate stability is controlled by pressure, temperature, gas content and pore water salinity (Sloan and Koh, 2007; Tishchenko et al., 2005). We calculated estimates for the base of the GHSZ (or BGHSZ) for each well location using the Colorado School of Mines Hydrate CSMHYD Program, an open source code available through the Colorado School of Mines which calculates a hydrate stability curve based on pressure, temperature, gas content and salinity (Sloan and Koh, 2007). For all calculations, we assume a pore water salinity of standard seawater, which is a reasonable assumption in near seafloor sedimentary systems that are not in a region with shallow salt. All other parameters are discussed below.

3.1.1. Geothermal Gradient

Accurately estimating the geothermal gradient at each well is essential for hydrate stability calculations. To estimate the geothermal gradient, both the seafloor temperature and temperature measurements below the seafloor are needed. For each well location, the seafloor temperature was estimated from water column temperature and depth data from the World Ocean Database (Boyer et al., 2013). For in-hole temperature measurements, bottomhole temperature (BHT) and true vertical bottomhole depth were acquired from the public well reports on the

Norwegian Petroleum Directorate website. The geothermal gradient was calculated using linear function between the seafloor and BHT.

BHT may underestimate true formation temperature because it measures the temperature of the drilling fluid at the bottom hole, which can be cooler than the surrounding sediment or rock (Evans and Coleman, 1974). BHT corrections can be applied (e.g. Peters and Nelson, 2012), but require multiple logging runs that record time and temperature or information such as effective thermal diffusivity of the bottomhole rock, which was not available in the existing dataset.

High-quality temperature measurements are recorded during a drill stem test (DST), where properties are measured in an interval that is packed off and allowed to flow over a period of time. This allows the borehole fluids more time to reach equilibrium with the surrounding formation (Peters and Nelson, 2012). In our dataset, five wells had publicly available DST data (Wells 6405/7-1, 6506/11-6, 6506/11-7, 7122/6-1, 7122/7-2). The difference between the geothermal gradient calculated with the DST vs. BHT was +3.3, +2.9, +0.1, +0.2, +12.4 ºC/km, respectively, with positive numbers meaning that the DST was warmer. Due to the generally low, though irregular difference between gradients calculated with DST and BHT, we chose not to apply any correction to the geothermal gradients calculated with BHT. If the geothermal gradient derived from the BHT is slightly lower, as may be the case, this produces a base of stability that is slightly deeper. For example, in Well 6405/7-1, the base of methane hydrate stability with a geothermal gradient of 41.0 ºC/km as estimated from the BHT is 374 m below seafloor (mbsf), while a DST calculated geothermal gradient of 44.3 ºC/km produces a methane hydrate base of stability of 347 mbsf.

In all wells where a DST was available, the geothermal gradient from the DST was used for hydrate stability calculations instead of the BHT data.

3.1.2. Gas Composition

Evidence strongly suggests that hydrate systems contain higher order hydrocarbon in the Barents Sea (Ostanin et al., 2013; Rajan et al., 2013; Vadakkepuliyambatta et al., 2017) and potentially on the Norwegian Margin (Hustoft et al., 2009). Therefore, the BGHSZ was calculated twice for each well, once assuming a pure methane gas composition and a second time using a gas composition with higher order hydrocarbons.

Due to differences in the data available, we used different hydrocarbon mixes in the Barents Sea and the Norwegian Margin. In the Barents Sea, only a few industry wells had gas measurements and almost all of these wells were missing crucial information on ethane and propane in the publicly available data. Therefore, we chose to use a local gas mix from Chand et al. (2008) and Vadakkepuliyambatta et al. (2017) of 96% methane, 3% ethane and 1% propane. When Vadakkepuliyambatta et al. (2017) used this gas mix, it closely matched the BSR depth within ~50 m in 12/35 locations in the Barents Sea and roughly matched the BSR depth within ~100 m in another 13/35 locations. Furthermore, Ostanin et al., (2013) estimated two higher-order gas mixes for the GHSZ above the Snøhvit gas field; the mix used herein is the more conservative of the two and produces a shallower base of stability and thinner GHSZ.

On the Norwegian Margin, ten wells in the dataset contained complete gas mix data. The shallowest gas measurements in each dataset were usually several hundred meters below the base of gas hydrate stability. Because the gas mix can change significantly with depth, we used the shallowest four gas mix measurements in each well to estimate an average gas mix as close as possible to the GHSZ: 91.6% methane, 2.3% ethane, 0.8% propane, and 4.1 % carbon dioxide.

3.2. Well Data Evaluation

Industry well log data is not of equal quality from well to well, and therefore, the dataset and well report for each well is evaluated individually.

On the well logs, the type of data and the quality of the data within both the methane and gas mix GHSZ are considered. All wells included in this dataset have at least 30 m of both gamma ray and resistivity well log data in the GHSZ. Some intervals have clearly erroneous data because of casing or pipe connections, and those intervals were not included in the hydrate evaluation, though well data outside those intervals was used in the evaluation. Some wells also have bulk density (ρ_b) and/or neutron porosity (ϕ_{neu}) well logs in the GHSZ. We categorize these wells with fair to high quality ρ_b and ϕ_{neu} data as Porosity wells and we have higher confidence in our gas hydrate analysis in these wells (see Supplementary Information).

The well report for each well was also consulted, and we recorded the orientation of the well (vertical or semi-vertical). The occurrence (or lack of) deeper gas or oil reservoirs was also noted, as well as the depth of the first observance of hydrocarbons in the well (see Supplementary Information).

3.3. Gas Hydrate Evaluation

Gas hydrate is an electrical insulator that increases measured resistivity when replacing more conductive brine in the pore space. Gas hydrate bearing intervals can be identified in resistivity data by an increase in resistivity relative to background water-saturated resistivity (Pearson et al., 1983; Goldberg et al., 2009; Waite et al., 2009). Depending on the type and quality of data available, background resistivity (R_o) can be either estimated or calculated.

3.3.1. Calculated Background Resistivity

When good- to high-quality ρ_b or ϕ_{neu} digital well logs are available, background resistivity can be calculated. Well log data may be edited slightly to remove intervals with significant drops in bulk density or significant increases in porosity; these intervals are likely affected by increases in hole size and are not related to gas hydrate occurrence. An example of log editing is shown in Figure 2, from Well 7219/9-1 in the Barents Sea. In this well, intervals with drops in bulk density were edited (black curve identified with arrows) to match the bulk density trends of surrounding layers.

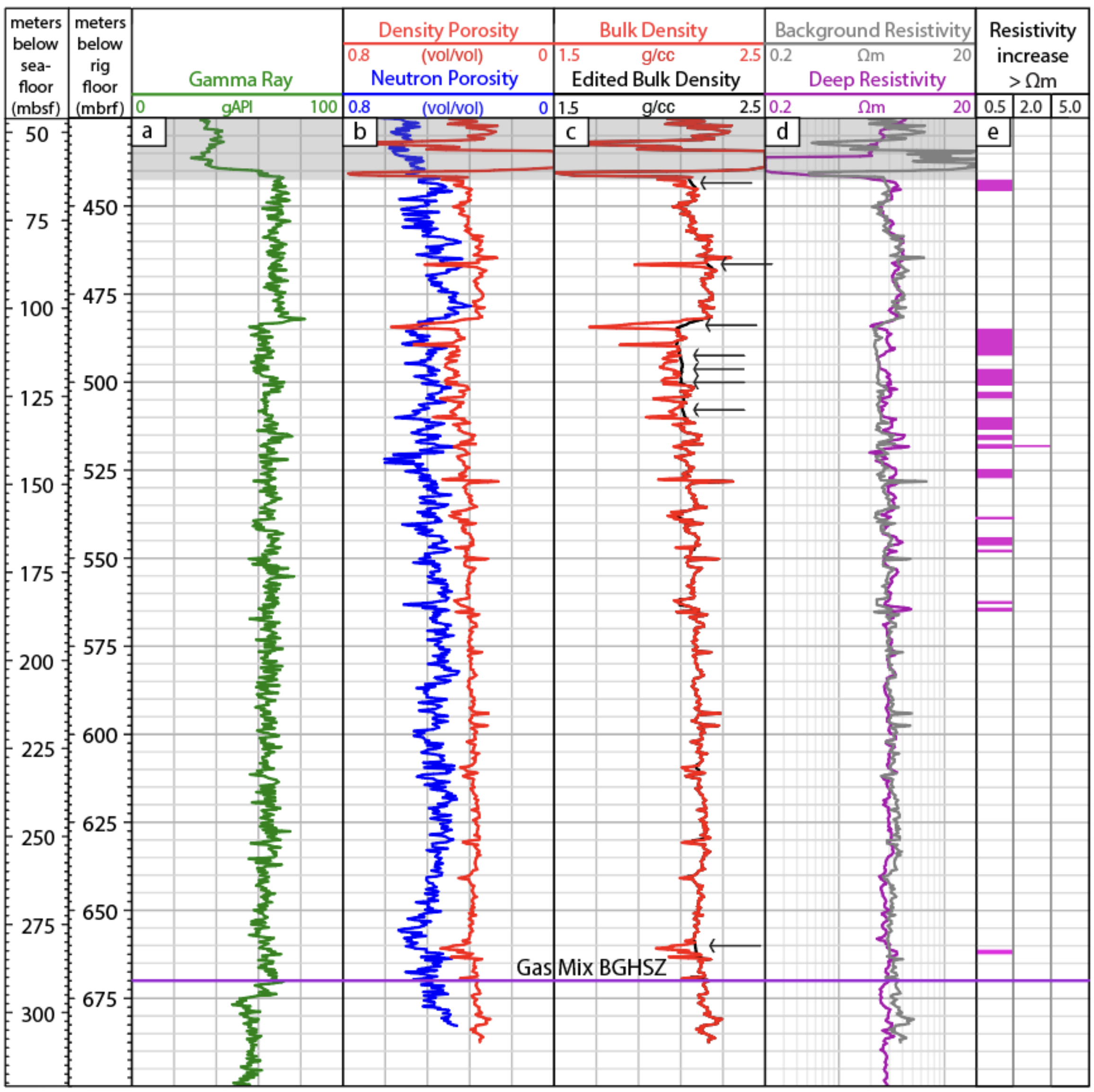

Figure 2. An example of gas hydrate evaluation using good quality industry well data from 7219/9-1 in the Barents Sea. The base of gas mix stability zone (BGHSZ) is indicated with a with a purple line; methane hydrate is not stable in 7219/9-1. Measured well log data used in the evaluation appears on Track a) gamma ray, b) neutron porosity, c) bulk density, and d) deep resistivity. Calculated and edited logs are also shown: b) calculated density porosity (Equation 1), c) edited bulk density and d) background resistivity, R_o (Equation 2). Black arrows identify

depths where there were significant edits made in the bulk density log. Track e shows the intervals that exceed 0.5, 2.0 and 5.0 Ωm based on the calculated R_o. Based on this analysis, this well is categorized as a C well (Table 2). The depth interval displayed is part of the Norland Group. BGHSZ = base of gas hydrate stability zone.

If ρ_b is used, porosity (ϕ) is calculated from bulk density assuming a sediment or rock grain density (ρ_g) of 2.7 g/cc and a pore water density (ρ_w) of 1.03 g/cc:

$$\phi_{den} = \frac{\rho_g - \rho_b}{\rho_g - \rho_w} \qquad \text{Equation 1}$$

Then either ϕ_{neu} or ϕ_{den} is applied as ϕ in Archie's porosity-resistivity equation to calculate background resistivity, R_o (Archie, 1942):

$$R_o = \frac{R_w}{\phi^m} \qquad \text{Equation 2}$$

where R_w is pore water resistivity, which we assume is the resistivity of seawater, R_w = 0.3 Ωm (Winsauer, 1952). For the cementation exponent, m, we apply an initial value of m = 2 (Jackson, 1978; Glover et al, 1997). If needed, the value of m is adjusted so that R_o matches the measured resistivity in intervals that are likely water saturated, as described in Malinverno et al. (2008). In Figure 2 Track d, we used m = 2 and the edited ϕ_{den} to calculate R_o for Well 7219/9-1.

3.3.2. Estimated Background Resistivity

If ϕ_{neu} or ρ_b logs are not available within the GHSZ or those logs are fair to poor quality, then R_o is estimated. In general, in high-porosity marine sediments, R_o does not change significantly between layers and is usually between 1-3 Ωm. Therefore, for wells from the Norwegian Margin, we estimate R_o using the borehole data in each well. To help avoid identifying intervals that are not hydrate bearing, we select a conservative R_o. This involves selecting not just the lowest resistivity, but a reasonable background trend within the GHSZ and just below the BGHSZ. For some wells, this includes selecting different background values for different intervals or an increasing R_o trend. An example of estimated R_o where more than one value was selected is shown in Figure 3 from Well 6302/6-1 on the Norwegian Margin. From 1365 m to 1736 m below rig floor (mbrf) or 79 to 450 m below seafloor (mbsf), we selected a R_o of 2.6 Ωm. Note that this background is not the lowest resistivity in this interval, but is a higher or more conservative R_o. Then, below 1736 mbrf (or 450 mbsf) a higher R_o of 3.1 Ωm was selected, as data below that interval and below the gas mix BGHSZ has a higher average resistivity.

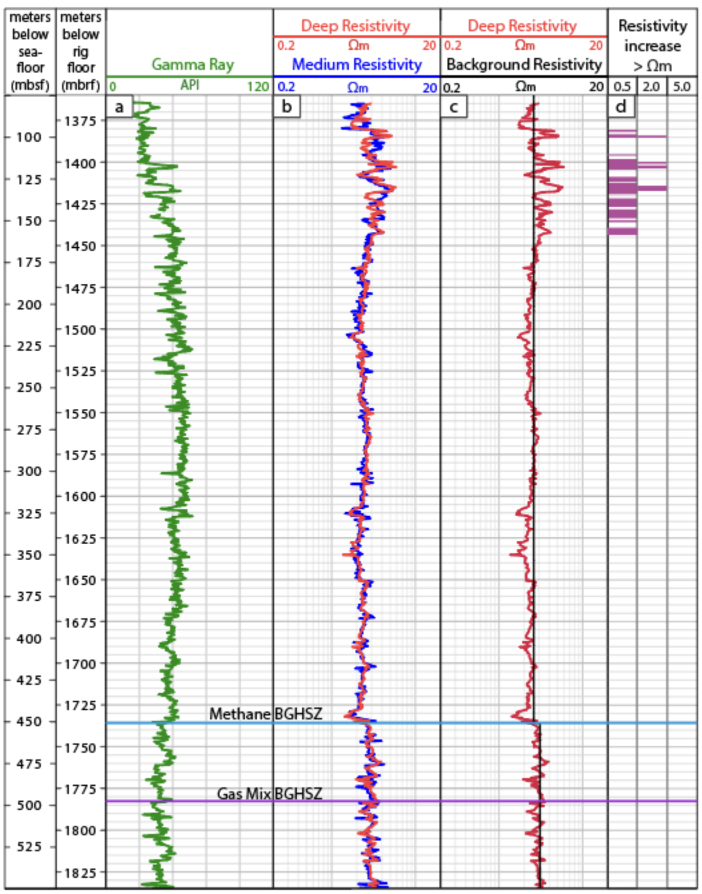

Figure 3. An example of gas hydrate evaluation where background resistivity is estimated using industry well data from 6302/6-1 on the Norwegian Margin. At this well, the methane BGHSZ (base of the gas hydrate stability zone) is shown in blue and the gas mix BGHSZ is shown in purple. Like many other wells in this dataset, this well has only gamma ray (Track a) medium resistivity and deep resistivity (Track b) within the gas hydrate stability zone. Track c shows the estimated background resistivity, which is based on the measured resistivity near and below the BGHSZ with the measured deep resistivity. Track d shows the intervals that exceed 0.5, 2.0 and

5.0 Ωm based on the estimated background resistivity. Based on this analysis, this well is categorized as a C well (Table 2).

In the Barents Sea near-seafloor lithologies are older and lithified, and the range of potential background resistivity was considerably higher. Therefore, we used wells where ϕ_{neu}, ρ_b or compressional velocity logs were available within or below the GHSZ to determine reasonable ranges for R_o in a particular formation (Table S1, Supplementary Information). The defined formation intervals for each well are available in the datasets from the Norwegian Petroleum Directorate.

3.4. Categorizing Hydrate Accumulations

After R_o is established, resistivity increases were categorized according to a set of criteria modified from Majumdar et al. (2017) (Table 1). In this scheme, A is the category representing a significant hydrate accumulation with the highest increase in resistivity, which is defined as a 5 Ωm increase above background for a total of 10 m. Note that the increase in resistivity can be distributed in smaller intervals through the GHSZ and does not have to be single layer of 10 m or greater. Resistivity increases and thickness are lower for B and C categories (Table 2). The D category represents the lowest increase in resistivity, 0.5 to 2 Ωm above background resistivity for less than 10 m total.

Table 1. Resistivity classification criteria for gas hydrate accumulations adapted from Majumdar et al. (2017). R_o = background resistivity.

Classification Criteria	Category
5 Ωm or more increase in resistivity above R_o for at least 10 m total	A
2 Ωm to 5 Ωm increase in resistivity above R_o for at least 10 m total, or more than 5 Ωm increase above R_o resistivity but less than 10 m	B
0.5 Ωm to 2 Ωm increase in resistivity above R_o for at least 10 m total; up to 5 Ωm increases for less than 10 m	C
0.5 Ωm to 2 Ωm increase above R_o resistivity for less than 10 m total	D
No resistivity increase greater than 0.5 Ωm above R_o	None

3.5. Hydrate Saturation

If high quality digital well log data is available, gas hydrate saturation, S_h, can be calculated using measured resistivity, R_m, R_o and Archie's saturation equation:

$$S_h = 1 - \left(\frac{R_o}{R_m}\right)^{\frac{1}{n}} \qquad \text{Equation 3}$$

where n is Archie's saturation exponent, set equal to 2.5 (Cook and Waite, 2018). We note, however, that there can be significant inaccuracies in the calculation of gas hydrate saturation. First, the most accurate saturations are calculated when a full suite of well logs and cores are available over the interval where saturation is calculated; in most cases, however, full datasets of this type are not common. In these industry datasets from Norway, the best datasets include fair to high quality bulk density and neutron porosity curves along with multiple resistivity logs.

The mode of hydrate occurrence also affects the accuracy of hydrate saturation. Usually, gas hydrate saturation can be calculated accurately using Equation 3 as long as the hydrate occurs in the primary pore space; this is the hydrate morphology commonly observed in sands or coarse silts (Kerkar et al., 2014). Gas hydrate in marine mud or clay, however, often occurs in near-vertical fractures that can result in high resistivity measurements due to electrical anisotropy and not because of a high saturation of hydrate (Cook et al., 2010). In this case gas hydrate saturation is usually significantly overestimated when using resistivity and Equation 3 and applying this equation directly should be avoided.

4. Results and Discussion

Based on the resistivity analysis and classification criteria we found evidence for gas hydrate in approximately half of industry boreholes offshore Norway (Figure 4, Table 2). From the publicly available well log data on the Norwegian Petroleum Directorate website and additional digital data, we identified 48 wells with quality well log data above the higher-order gas mix base of hydrate stability. When a gas mix is used to determine the base of stability, 10 out of 18 wells in the Barents Sea and 15 out of 30 wells on the Norwegian Margin have evidence for gas hydrate (Figure 4, Table 2). If only pure methane gas composition is used to determine the base of stability, there are only 24 wells with quality well log data in the GHSZ, as methane hydrate has a more limited range of stability than higher-order gas mixes. With the methane only base of stability we found evidence for gas hydrate in 0 out of 3 wells in the Barents Sea and 11 out of 21 wells Norwegian Sea (Figure 4, Table 2).

Table 2. The number of wells in the Barents Sea and Norwegian Margin that fall into each resistivity ranked category (Table 1); wells in Category A have significant hydrate accumulation with the highest increase in resistivity and each category below that has a lower increases in resistivity and/or a reduced thickness. The number of wells on each margin is further separated by the two estimates of the base of the gas hydrate stability zone (BGHSZ): the designated gas mix for each margin or a methane-only mix.

	Barents Sea		Norwegian Margin	
Hydrate Category	Gas Mix BGHSZ	Methane BGHSZ	Gas Mix BGHSZ	Methane BGHSZ
A	0	0	0	0
B	0	0	2	1
C	5	0	10	7
D	5	0	3	3
No Hydrate	8	3	15	10
Total & Percent with Hydrate	10/18 55.6%	0/3 0.0%	15/30 50.0%	11/21 61.1%

4.1. Gas hydrate accumulations

In general, in both the Barents Sea and the Norwegian Margin, gas hydrate accumulations are associated with low resistivity measurements with an increase of 0.5 and 2.0 Ωm above R_o, as shown by the predominance of C and D wells in the dataset (Table 3, Figures 2-4). Only two wells are ranked in Category B, which means they have at more than a 2 Ωm increase above background.

Category B Well 6706/11-1 in the Norwegian Sea, has high quality well log data, additional porosity well logs ($\boldsymbol{\phi_{neu}}$ and $\boldsymbol{\rho_b}$) logs in the gas hydrate stability zone and strong evidence for hydrate in both the methane and gas mix GHSZ (Figure 5). In Well 6706/11-1, we use $\boldsymbol{\phi_{neu}}$ to calculate R_o (Equation 2) and identify hydrate-bearing intervals as $\boldsymbol{\phi_{neu}}$ log in this well has more consistent, reasonable porosity measurements that have a somewhat similar trend to the deep resistivity measurement. In this well, we find hydrate primary concentrated **in a thick interval** between 134**1** and 14**19** mbrf (77 and 155 mbsf), as indicated by increases in resistivity between 2 and 5 Ωm above R_o. Based on Equation 3, this corresponds to a hydrate saturation of ~20-30%. However, this calculation should be considered with caution, as the gamma ray in this interval is ~70 API, which is too high for most sands or coarse silts and implies that this interval likely contains a significant clay fraction; this may mean hydrate is forming in fractures or lenses where Archie's saturation equation is not applicable. The other Category B well is displayed in Supplementary Information.

Similar to Figures 2, 3, and 5, we observe hydrate accumulations in intervals ranging from tens of centimeters to tens of meters; it is likely that some of these intervals are thinner than true hydrate accumulations given that we select R_o conservatively and require an increase of 0.5 to count a layer as gas hydrate bearing. We also observe that gas hydrate was generally distributed in discrete intervals in the middle of the gas hydrate stability zone. This observation is partly biased by the fact that the first ~25 meters below seafloor (mbsf) is almost always missing because jet-in casing is set at the top of the hole, and therefore, if gas hydrate occurs in that near seafloor interval, it cannot be observed. Even so, an important observation is that gas hydrate is not commonly observed near the base of the GHSZ whether it is defined based on the stability in a pure methane or mixed gas system.

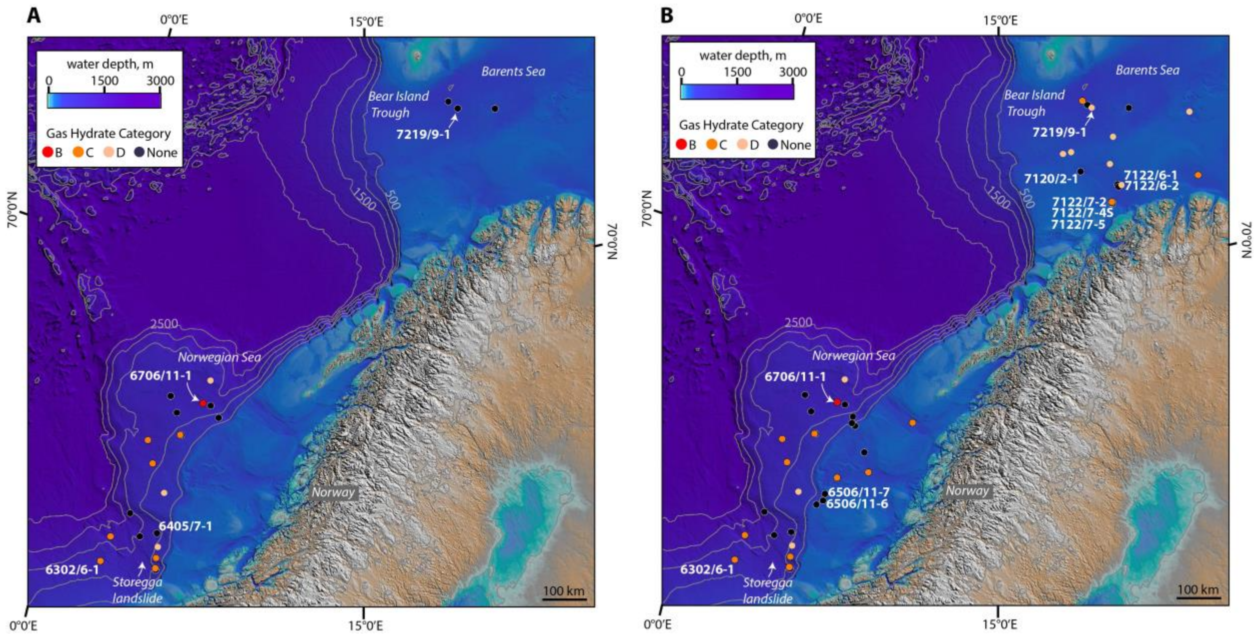

Figure 4. The location and gas hydrate category (Table 1) of wells in the Barents and Norwegian Sea assuming a) methane hydrate stability and b) a mix of higher order hydrocarbons in the hydrate stability zone.

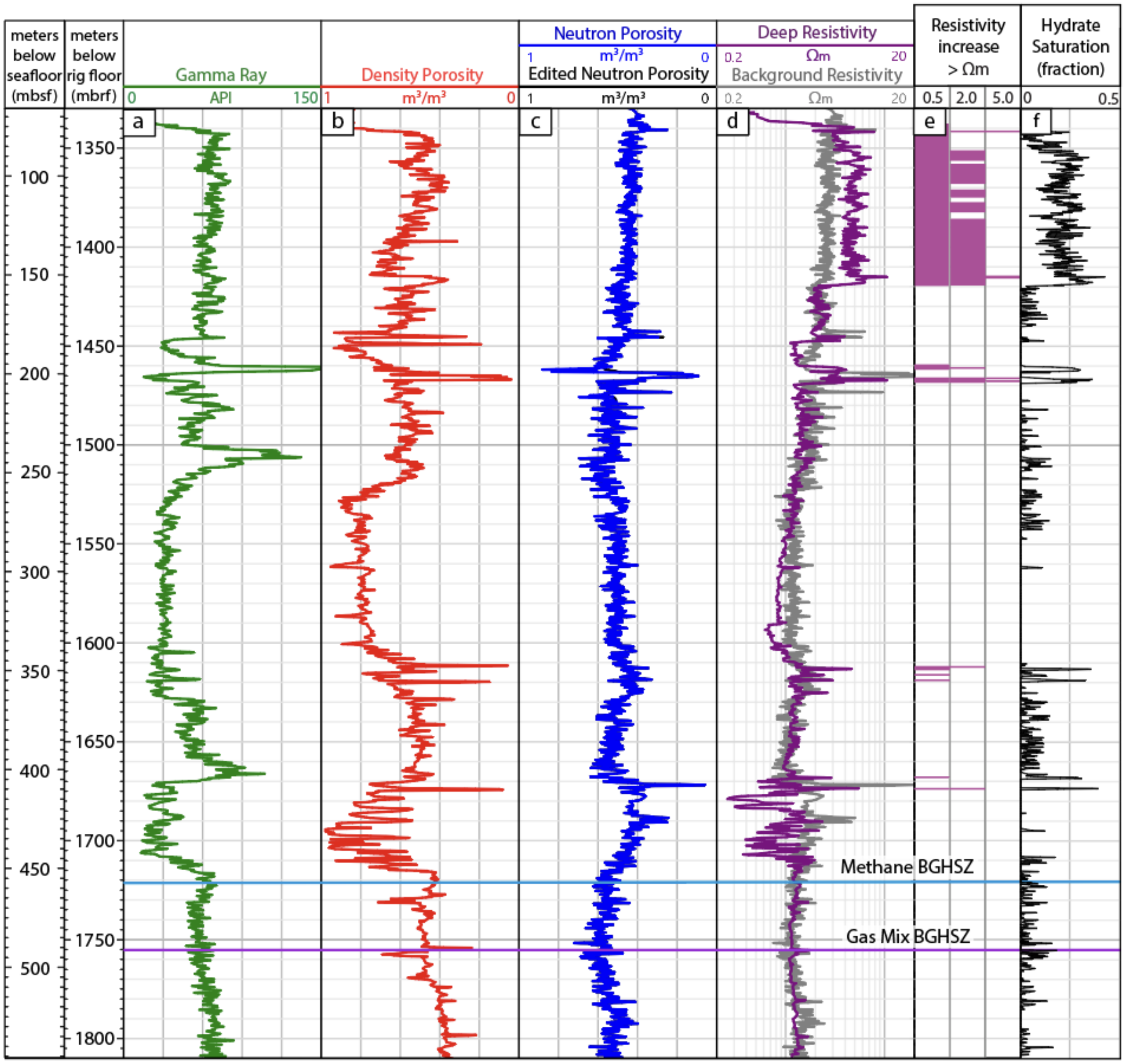

Figure 5. The industry well with the most significant hydrate accumulation in this the dataset, Well 6706/11-1 in the Norwegian Sea. Measured well log data appears on Track a) gamma ray, c) neutron porosity and d) deep resistivity. Calculated and edited logs are also shown: b) calculated density porosity (Equation 1), c) edited neutron porosity, d) background resistivity, R_o (Equation 2), and f) gas hydrate saturation (Equation 3). Track e shows the intervals that exceed 0.5, 2.0 and 5.0 Ωm based on the calculated R_o; this well is categorized as a B well. BGHSZ = base of gas hydrate stability zone.

4.2. The connection to deeper hydrocarbon reservoirs

The source of the gas bound in gas hydrate systems is an open and important scientific question (Ruppel and Kessler, 2017; You et al., 2019). In most locations, there are two endmember gas sources: thermogenic gas from deeper oil and gas reservoirs or shallow microbial gas generated from the consumption of organic matter within or near the GHSZ. Hydrate systems may have a single source, a mixture of both sources, and may also contain microbially reworked thermogenic gas. Understanding the source of the gas in hydrate systems will enhance our ability to estimate the influence of hydrate in the carbon cycle and improve the remote detection of hydrate systems.

With this dataset, we have the unique opportunity to look at the relationship between shallow gas hydrate systems and the occurrence of deeper oil and gas reservoirs. The intervals evaluated in the GHSZ in each well lie directly above any deeper oil and gas targets. Most wells in the dataset are oriented vertically, and five wells in the Barents Sea have a semi-vertical orientation with lateral deviations up to 1 km. All semi-vertical wells, however, still lie above the identified mapped area of the oil or gas reservoir, when one was found. No wells deviate onto another reservoir.

We used the available reports on the Norwegian Petroleum Directorate website to divide the wells into two categories: hydrocarbon reservoir or no hydrocarbon reservoir. If producible hydrocarbons were encountered in the well, we noted the top depth of the hydrocarbon accumulation and categorized the well as having a hydrocarbon reservoir. If the well was listed as dry or only containing a trace amount of hydrocarbon (called a 'show') it is categorized a no hydrocarbon reservoir. It is possible that these trace hydrocarbons were once significant oil and gas reservoirs, but it is also possible that they never were. In any case, hydrocarbon shows are not currently significant hydrocarbon reservoirs that could form a buoyant phase and leak or advect into shallower rocks and sediment. For this reason, we choose to categorized these as non-hydrocarbon reservoirs. We also note that none of the hydrocarbon reservoirs or hydrocarbon shows were within the GHSZs.

Using these categories, we find no relationship between the presence of hydrate and the occurrence of a deeper oil and gas reservoir in either the Barents Sea or the Norwegian Margin (Figure 6). Wells with evidence for hydrate are just as likely (if not slightly more so) to occur above no hydrocarbon reservoir than to occur above a producible hydrocarbon reservoir. The reverse also holds true: wells with no evidence for hydrate are just as likely to occur above a producible hydrocarbon reservoir than no hydrocarbon reservoir. Notably, the well with the most significant hydrate accumulation in the dataset, 6706/11-1 (Figure 5), is a dry hole with no hydrocarbon shows.

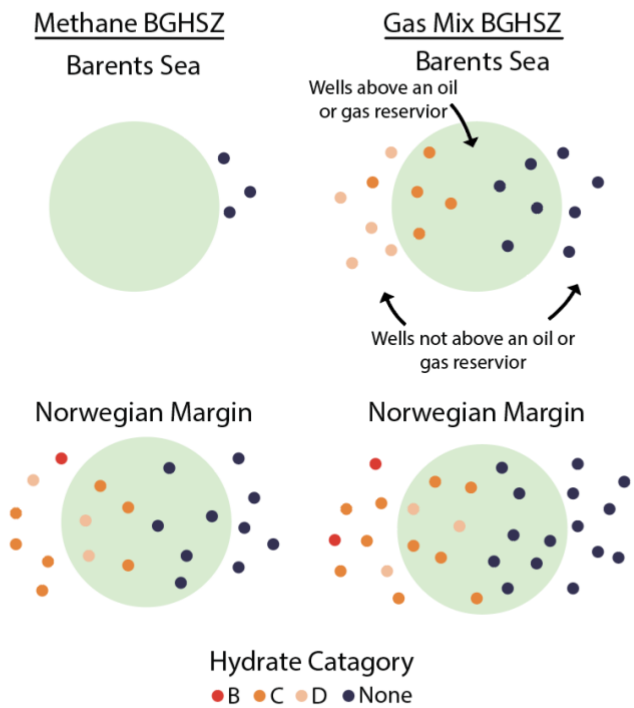

Figure 6. A cartoon showing the wells, their hydrate category (Table 1) and their relationship to a deeper oil or gas reservoirs. Wells above the green circle lie above an oil or gas reservoir and wells outside the green circle do not. The wells are divided into four different scenarios based on the location, either Barents Sea or Norwegian Margin, and the estimated base of hydrate stability, either methane only or the margin-specific gas mix. A figure showing these results is available in the Supplementary Information and the results for each well are archived in the dataset spreadsheet.

Of course, the local geologic conditions influence fluid flow and shallow gas source near each well. For example, on the Norwegian Margin, there is strong evidence for shallow free gas within and near the gas hydrate stability zone on 2D seismic and ocean bottom seismometer surveys (Mienert et al., 2005a). Above the Ormen Lange field, 2 out of 3 wells had evidence for hydrate, which may suggest that these two wells could be sourced from the deeper gas field. Of course, it may also be that the shallow free gas above the Ormen Lange field doesn't have a connection to the deeper gas reservoir; there are no gas samples available from these shallow gas and hydrate accumulations to verify the origin. Thus, even when more detailed scientific datasets like seismic data and ocean bottom seismometer surveys exist, questions of gas source cannot be fully answered.

Therefore, while we acknowledge that local geological conditions can certainly influence natural gas flow, fluid flow and the accumulation of gas hydrate (e.g. You et al., 2019), we argue that this dataset should be considered holistically as detailed geophysical and geochemical datasets needed to fully characterize the gas hydrate system are not available at every site.

4.3. The background gas hydrate system

Most industry wells are drilled away from shallow high amplitudes observed in seismic data that may indicate shallow gas or gas hydrate, because these amplitudes can also signify dangerous and expensive to mitigate overpressured intervals. Therefore, our results from industry wells provide a picture of background gas hydrate systems that are drilled away from shallow high amplitudes.

Three of the key results from this study suggest that background hydrate systems in both the Norwegian Margin and the Barents Sea are not primarily sourced from deeper thermogenic oil and gas reservoirs: 1) the commonly occurring though relatively low resistivity increases above R_o (Table 2), which suggests the mechanism for gas transport is very low or intermittent fluid flux or a diffusive migration of gas, 2) the observation that most gas hydrate occurs in the middle of the GHSZ (i.e. Figures 2, 3, and 5), away from the BGHSZ suggesting gas is not primarily sourced from below and 3) the lack of distinct association between observed hydrate accumulations and deeper oil and gas reservoirs (Figure 6).

Malinverno (2011) hypothesized that thin, coarse-sand or silt layers are slowly filled with hydrate via methane transported by diffusion in the dissolved phase. In what is termed short migration or diffusive migration, methane is generated by microbes within organic rich clays and then transported short distances (cm to m) via diffusion to coarser sand or silt layers (Malinverno, 2011). In coarser sediments, there is a lower threshold for methane solubility meaning that hydrate forms in these sediments first. Once hydrate forms in the coarser sediment, this results in a continuous, slow diffusive flux of methane from organic-rich clays into the coarser sediments. This process has now been modeled or invoked at a number of locations to explain hydrate accumulations in thin sands (cm to a few meters thick) that are not close to the base of hydrate stability or a clear methane migration pathway, including the northern Gulf of Mexico (Cook and Malinverno, 2013; Nole et al., 2017; Wei et al., 2019), the Hikurangi Margin, New Zealand (Cook et al., 2020), the Andaman Islands (Malinverno and Goldberg, 2015), and the South China Sea (Guan et al., 2021). A somewhat similar diffusive migration of methane may also fill and propagate hydrate filled fractures in clays (Oti et al., 2019). Because nearly all the hydrate accumulations in the Barents and Norwegian Sea are found to be significantly above the base of hydrate stability with relatively low increases in resistivity (indicating low saturation or concentration) and not linked to deeper oil and gas reservoirs, we argue that diffusive migration is likely the main mechanism for gas transport and hydrate accumulation in background gas hydrate systems offshore Norway.

In the Barents Sea, a microbial gas source may seem somewhat contradictory as we previously noted that there is strong evidence for higher-order hydrocarbons in the shallow interval that coincides with the GHSZ (Ostanin et al., 2013; Rajan et al., 2013; Vadakkepuliyambatta et al., 2017). However, a concentration of only 1 or 2% higher order hydrocarbon is needed to significantly increase the base of hydrate stability. While the data herein suggests that thermogenic gas is not a primary source for background gas hydrate systems at the locations analyzed herein, it may be enough of a secondary source to significantly increase the thickness of the gas hydrate stability zone. In addition, the Barents Sea also has two unique features that may allow for possible diffusion of higher-order hydrocarbons from a thermogenic source: 1) thermogenic reservoirs are much closer to the hydrate stability zone (sometimes only a few hundred meters away) and 2) relatively shallow rocks are significantly older (50-100 Ma) meaning that there may be enough time for diffusion to take place.

Another possibility that can explain the microbial source implied in this dataset and previous publications suggesting thermogenic source gas is that different hydrate systems may have different primary sources of gas offshore Norway. In this case, hydrate systems would have thermogenic source gas when strong amplitudes and migration pathways are visible on seismic data and microbial source gas for background systems that do not have strong amplitudes or clear migration pathways on seismic data. Scientific ocean drilling is needed to collect gas samples throughout and below the GHSZ in gas hydrate systems with a range of seismic signatures to clearly resolve the gas sourcing in these systems.

5. Conclusions

We analyze publicly available well logs from the Barents Sea and mid-Norwegian Margin and find approximately 50% of well have evidence for gas hydrate in the gas hydrate stability zone, suggesting gas hydrate is pervasive across offshore Norway. We observe that these hydrate accumulations are usually associated with relatively low increases in resistivity, which suggests low saturation or low concentration gas hydrate. In addition, we observe that these accumulations are almost always significantly above the estimated base of hydrate stability. When we compare the dataset of wells analyzed for gas hydrate, we find no association between gas hydrate occurrence and deeper oil and gas reservoirs, suggesting that these deeper oil and gas sources are not the main gas source for gas hydrate systems. Based on this evidence, we infer that gas hydrate accumulations at the industry well locations studied herein are most likely microbial in origin.

Acknowledgments, Samples, and Data

This research was funded by NSF Award number #1752882. We thank Schlumberger for their donation of TechLog to Ohio State University, which was used for log analysis. We thank the editor and two reviewers for their helpful comments. Well log, drilling data and reservoir maps can be obtained on the Norwegian Petroleum Directorate (https://factpages.npd.no/en/wellbore/pageview/exploration/all). The compiled dataset for this project is available and archived at: https://www.marine-geo.org/tools/search/Files.php?data_set_uid=29783

Andreassen, K., Hubbard, A., Winsborrow, M., Patton, H., Vadakkepuliyambatta, S., Plaza-Faverola, A., Gudlaugsson, E., Serov, P., Deryabin, A., Mattingsdal, R., Mienert, J., Bünz, S., 2017. Massive blow-out craters formed by hydrate-controlled methane expulsion from the Arctic seafloor. Science (1979) 356, 948–953. https://doi.org/10.1126/science.aal4500

Archer, D., 2007. Methane hydrate stability and anthropogenic climate change. Biogeosciences 4, 993–1057. https://doi.org/10.5194/bgd-4-993-2007

Archie, G.E., 1942. The electrical resistivity log as an aid in determining some reservoir characteristics, in: Transactions of the American Institute of Mining and Metallurgical Engineers, Vol. 146. pp. 54–63.

Barnes, P.M., Pecher, I.A., LeVay, L.J., Bourlange, S.M., Brunet, M.M.Y., Cardona, S., Clennell, M.B., Cook, A.E., Crundwell, M.P., Dugan, B., Elger, J., Gamboa, D., Georgiopoulou, A., Greve, A., Han, S., Heeschen, K.U., Hu, G., Kim, G.Y., Kitajima, H., Koge, H., Li, X., Machado, K.S., McNamara, D.D., Moore, G.F., Mountjoy, J.J., Nole, M.A., Owari, S., Paganoni, M., Petronotis, K.E., Rose, P.S., Screaton, E.J., Shankar, U., Shepherd, C.L., Torres, M.E., Underwood, M.B., Wang, X., Woodhouse, A.D., Wu, H.-Y., 2019. Site U1517 372. https://doi.org/10.14379/iodp.proc.372a.103.2019

Boswell, R., Collett, T.S., 2011. Current perspectives on gas hydrate resources. Energy Environ Sci 4, 1206. https://doi.org/10.1039/c0ee00203h

Boyer, T.P., Antonov, J.I., Baranova, O.K., Coleman, C., Garcia, H.E., Grodsky, A., Johnson, D.R., Locarnini, R.A., Mishonov, A. v., O'Brien, T.D., Paver, C.R., Reagan, J.R., Seidov, D., Smolyar, I. v., Zweng, M.M., 2013. 2013: World Ocean Database 2013, NOAA Atlas NESDIS 72. Silver Spring, Maryland. https://doi.org/http://doi.org/10.7289/V5NZ85MT

Brekke, H., 2000. The tectonic evolution of the Norwegian Sea continental margin with emphasis on the Voring and More Basins, Geological Society Special Publication. https://doi.org/10.1144/GSL.SP.2000.167.01.13

Bryn, P., Berg, K., Forsberg, C.F., Solheim, A., Kvalstad, T.J., 2005. Explaining the Storegga Slide. Mar Pet Geol 22, 11–19. https://doi.org/10.1016/j.marpetgeo.2004.12.003

Bugge, T., Befring, S., Belderson, R.H., Eidvin, T., Jansen, E., Kenyon, N.H., Holtedahl, H., Sejrup, H.P., 1987. A giant three-stage submarine slide off Norway. Geo-Marine Letters 7, 191–198. https://doi.org/10.1007/BF02242771

Bünz, S., Mienert, J., Berndt, C., 2003. Geological controls on the Storegga gas-hydrate system of the mid-Norwegian continental margin. Earth Planet Sci Lett 209, 291–307. https://doi.org/10.1016/S0012-821X(03)00097-9

Bünz, S., Mienert, J., Vanneste, M., Andreassen, K., 2005. Gas hydrates at the Storegga Slide: Constraints from an analysis of multicomponent, wide-angle seismic data. Geophysics 70, 19–34. https://doi.org/10.1190/1.2073887

Collett, T.S., Boswell, R., Waite, W.F., Kumar, P., Roy, S.K., Chopra, K., Singh, S.K., Yamada, Y., Tenma, N., Pohlman, J., Zyrianova, M., 2019. India National Gas Hydrate Program Expedition 02 Summary of Scientific Results: Gas hydrate systems along the eastern continental margin of India. Mar Pet Geol 108, 39–142. https://doi.org/10.1016/j.marpetgeo.2019.05.023

Cook, A.E., Anderson, B.I., Malinverno, A., Mrozewski, S., Goldberg, D., 2010. Electrical anisotropy due to gas hydrate-filled fractures. Geophysics 75, 173–185. https://doi.org/10.1190/1.3506530

Cook, A.E., Malinverno, A., 2013. Short migration of methane into a gas hydrate-bearing sand layer at Walker Ridge, Gulf of Mexico. Geochemistry, Geophysics, Geosystems 14, 283–291. https://doi.org/10.1002/ggge.20040

Cook, A.E., Paganoni, M., Clennell, M.B., McNamara, D.D., Nole, M., Wang, X., Han, S., Bell, R.E., Solomon, E.A., Saffer, D.M., Barnes, P.M., Pecher, I.A., Wallace, L.M., LeVay, L.J., Petronotis, K.E., 2020. Physical Properties and Gas Hydrate at a Near-Seafloor Thrust Fault, Hikurangi Margin, New Zealand. Geophys Res Lett 47, 1–11. https://doi.org/10.1029/2020GL088474

Cook, A.E., Waite, W.F., 2018. Archie's Saturation Exponent for Natural Gas Hydrate in Coarse-Grained Reservoirs. J Geophys Res Solid Earth 123. https://doi.org/10.1002/2017JB015138

Doré, A.G., Lundin, E.R., 1996. Cenozoic compressional structures on the NE Atlantic margin: Nature, origin and potential significance for hydrocarbon exploration. Petroleum Geoscience 2, 299–311. https://doi.org/10.1144/petgeo.2.4.299

Evans, T.R., Coleman, N.C., 1974. North Sea Geothermal Gradients. Nature 247, 28–30.

Faleide, J.I., Gudlaugsson, S.T., Jacquart, G., 1984. Evolution of the western Barents Sea. Mar Pet Geol 1, 70–78. https://doi.org/10.1016/0264-8172(84)90082-5

Ferré, B., Mienert, J., Feseker, T., 2012. Ocean temperature variability for the past 60 years on the Norwegian-Svalbard margin influences gas hydrate stability on human time scales. J Geophys Res Oceans 117, 1–14. https://doi.org/10.1029/2012JC008300

Flemings, P.B., Phillips, S.C., Boswell, R., Collett, T.S., Cook, A.E., Dong, T., Frye, M., Goldberg, D.S., Guerin, G., Holland, M.E., Jang, J., Meazell, K., Morrison, J., O'Connell, J.I., Petrou, E.G., Pettigrew, T., Polito, P.J., Portnov, A., Santra, M., Schultheiss, P.J., Seol, Y., Shedd, W., Solomon, E.A., Thomas, C.M., Waite, W.F., You, K., 2020. Pressure coring a Gulf of Mexico deep-water turbidite gas hydrate reservoir: Initial results from The University of Texas–Gulf of Mexico 2-1 (UT-GOM2-1) Hydrate Pressure Coring Expedition. Am Assoc Pet Geol Bull 104, 1847–1876. https://doi.org/10.1306/05212019052

Goldberg, D.S., Kleinberg, R.L., Weinberger, J.L., Malinverno, A., McLellan, P.J., Collett, T.S., 2010. 16. Evaluation of Natural Gas-Hydrate Systems Using Borehole Logs. Geophysical Characterization of Gas Hydrates 239–261. https://doi.org/10.1190/1.9781560802197.ch16

Gorman, A.R., Senger, K., 2010. Defining the updip extent of the gas hydrate stability zone on continental margins with low geothermal gradients. J Geophys Res Solid Earth 115. https://doi.org/10.1029/2009JB006680

Guan, J., Cong, X., Archer, D.E., Wan, L., Liang, D., 2021. Spatio-temporal evolution of stratigraphic-diffusive methane hydrate reservoirs since the Pliocene along Shenhu continental slope, northern South China sea. Mar Pet Geol 125. https://doi.org/10.1016/j.marpetgeo.2020.104864

Haacke, R.R., Westbrook, G.K., Hyndman, R.D., 2007. Gas hydrate, fluid flow and free gas: Formation of the bottom-simulating reflector. Earth Planet Sci Lett 261, 407–420. https://doi.org/10.1016/j.epsl.2007.07.008

Hustoft, S., Dugan, B., Mienert, J., 2009. Effects of rapid sedimentation on developing the Nyegga pockmark field: Constraints from hydrological modeling and 3-D seismic data, offshore mid-Norway. Geochemistry, Geophysics, Geosystems 10. https://doi.org/10.1029/2009GC002409

Hustoft, S., Mienert, J., Bünz, S., Nouzé, H., 2007. High-resolution 3D-seismic data indicate focussed fluid migration pathways above polygonal fault systems of the mid-Norwegian margin. Mar Geol 245, 89–106. https://doi.org/10.1016/j.margeo.2007.07.004

Ivanov, M., Westbrook, G.K., Blinova, V., Kozlova, E., Mazzini, A., Nouzé, H., Minshull, T.A., 2007. First sampling of gas hydrate from the Vøring plateau. Eos (Washington DC) 88, 1–4. https://doi.org/10.1029/2007EO190001

Kerkar, P.B., Horvat, K., Jones, K.W., Mahajan, D., 2014. Imaging methane hydrates growth dynamics in porous media using synchrotron X-ray computed tomography. Geochemistry Geophysics Geosystems 15, 4759–4768. https://doi.org/10.1002/2014GC005373

Laberg, J., Andreassen, K., Knutsen, S.M., 1998. Inferred gas hydrate on the Barents Sea shelf - A model for its formation and a volume estimate. Geo-Marine Letters 18, 26–33. https://doi.org/10.1007/s003670050048

Laberg, J.S., Dahlgren, T., Vorren, T.O., Haflidason, H., Bryn, P., 2001. Seismic analyses of cenozoic contourite drift development in the Northern Norwegian Sea. Marine Geophysical Research 22, 401–416. https://doi.org/10.1023/A:1016347632294

Lasabuda, A.P.E., Johansen, N.S., Laberg, J.S., Faleide, J.I., Senger, K., Rydningen, T.A., Patton, H., Knutsen, S.M., Hanssen, A., 2021. Cenozoic uplift and erosion of the Norwegian Barents Shelf – A review. Earth Sci Rev. https://doi.org/10.1016/j.earscirev.2021.103609

Loeng, H., 1991. Features of the physical oceanographic conditions of the Barents Sea. Polar Res 10, 5–18. https://doi.org/10.1111/j.1751-8369.1991.tb00630.x

Majumdar, U., Cook, A.E., Scharenberg, M., Burchwell, A., Ismail, S., Frye, M., Shedd, W., 2017. Semi-quantitative gas hydrate assessment from petroleum industry well logs in the northern Gulf of Mexico. Mar Pet Geol 85, 233–241. https://doi.org/10.1016/j.marpetgeo.2017.05.009

Malinverno, A., 2010. Marine gas hydrates in thin sand layers that soak up microbial methane. Earth Planet Sci Lett 292, 399–408. https://doi.org/10.1016/j.epsl.2010.02.008

Malinverno, A., Goldberg, D.S., 2015. Testing short-range migration of microbial methane as a hydrate formation mechanism: Results from Andaman Sea and Kumano Basin drill sites and global implications. Earth Planet Sci Lett 422, 105–114. https://doi.org/10.1016/j.epsl.2015.04.019

Malinverno, A., Kastner, M., Torres, M.E., Wortmann, U.G., 2008. Gas hydrate occurrence from pore water chlorinity and downhole logs in a transect across the northern Cascadia margin (Integrated Ocean Drilling Program Expedition 311). J Geophys Res Solid Earth 113, 1–18. https://doi.org/10.1029/2008JB005702

Martinsen, O.J., Lien, T., Jackson, C., 2005. Cretaceous and Palaeogene turbidite systems in the North Sea and Norwegian Sea basins: Source, staging area and basin physiography controls on reservoir development. Petroleum Geology Conference Proceedings 6, 1147–1164. https://doi.org/10.1144/0061147

Maslin, M., Owen, M., Betts, R., Day, S., Dunkley Jones, T., Ridgwell, A., 2010. Gas hydrates: past and future geohazard? Philosophical Transactions of the Royal Society A: Mathematical, Physical and Engineering Sciences 368, 2369–2393. https://doi.org/10.1098/rsta.2010.0065

Mienert, J., Bünz, S., Guidard, S., Vanneste, M., Berndt, C., 2005. Ocean bottom seismometer investigations in the Ormen Lange area offshore mid-Norway provide evidence for shallow gas layers in subsurface sediments. Mar Pet Geol 22, 287–297. https://doi.org/10.1016/j.marpetgeo.2004.10.020

Mienert, J., Posewang, J., Baumann, M., 1998. Gas hydrates along the northeastern Atlantic margin: possible hydrate- bound margin instabilities and possible release of methane. Geol Soc Spec Publ 137, 275–291. https://doi.org/10.1144/GSL.SP.1998.137.01.22

Minshull, T.A., Marín-Moreno, H., Betlem, P., Bialas, J., Bünz, S., Burwicz, E., Cameselle, A.L., Cifci, G., Giustiniani, M., Hillman, J.I.T., Hölz, S., Hopper, J.R., Ion, G., León, R., Magalhaes, V., Makovsky, Y., Mata, M.P., Max, M.D., Nielsen, T., Okay, S., Ostrovsky, I., O'Neill, N., Pinheiro, L.M., Plaza-Faverola, A.A., Rey, D., Roy, S., Schwalenberg, K., Senger, K., Vadakkepuliyambatta, S., Vasilev, A., Vázquez, J.T., 2020. Hydrate occurrence in Europe: A review of available evidence. Mar Pet Geol 111, 735–764. https://doi.org/10.1016/j.marpetgeo.2019.08.014

Nixon, F.C., Chand, S., Thorsnes, T., Bjarnadóttir, L.R., 2019. A modified gas hydrate-geomorphological model for a new discovery of enigmatic craters and seabed mounds in the Central Barents Sea, Norway. Geo-Marine Letters 39, 191–203. https://doi.org/10.1007/s00367-019-00567-1

Nole, M., Daigle, H., Cook, A.E., Hillman, J.I.T., Malinverno, A., 2017. Linking basin-scale and pore-scale gas hydrate distribution patterns in diffusion-dominated marine hydrate systems. Geochemistry, Geophysics, Geosystems 18. https://doi.org/10.1002/2016GC006662

NPD, 2014. Lithostratigraphic Chart Norwegian Barents Sea.

Ostanin, I., Anka, Z., di Primio, R., Bernal, A., 2013. Hydrocarbon plumbing systems above the Snøhvit gas field: Structural control and implications for thermogenic methane leakage in the Hammerfest Basin, SW Barents Sea. Mar Pet Geol 43, 127–146. https://doi.org/10.1016/j.marpetgeo.2013.02.012

Oti, E.A., Cook, A.E., Welch, S.A., Sheets, J.M., Crandall, D., Rose, K., Daigle, H., 2019. Hydrate-filled Fracture Formation at Keathley Canyon 151, Gulf of Mexico, and Implications for Non-vent Sites. Geochemistry, Geophysics, Geosystems 20, 4723–4736. https://doi.org/10.1029/2019GC008637

Pape, T., Feseker, T., Kasten, S., Fischer, D., Bohrmann, G., 2011. Distribution and abundance of gas hydrates in near-surface deposits of the Håkon Mosby Mud Volcano, SW Barents Sea. Geochemistry, Geophysics, Geosystems 12, 1–22. https://doi.org/10.1029/2011GC003575

Peters, K.E., Nelson, P.H., 2012. Criteria to Determine Borehole Formation Temperatures for Calibration of Basin and Petroleum System Models, in: Harris, N.B., Peters, K.E. (Eds.), . SEPM (Society for Sedimentary Geology), p. 219.

Phrampus, B.J., Hornbach, M.J., 2012. Recent changes to the Gulf Stream causing widespread gas hydrate destabilization. Nature 490, 527–530. https://doi.org/10.1038/nature11528

Rajan, A., Bünz, S., Mienert, J., Smith, A.J., 2013. Gas hydrate systems in petroleum provinces of the SW-Barents Sea. Mar Pet Geol 46, 92–106. https://doi.org/10.1016/j.marpetgeo.2013.06.009

Rise, L., Bellec, V.K., Ch, S., Bøe, R., 2014. Pockmarks in the southwestern Barents Sea and Finnmark fjords. Norsk Geologisk Tidsskrift 94, 263–282. https://doi.org/10.17850/njg94-4-02

Ruppel, C., Kessler, J.D., 2017. The Interaction of Climate Change and Methane Hydrates. Reviews of Geophysics 1–43. https://doi.org/10.1002/2016RG000534

Serov, P., Vadakkepuliyambatta, S., Mienert, J., Patton, H., Portnov, A., Silyakova, A., Panieri, G., Carroll, M.L., Carroll, J.L., Andreassen, K., Hubbard, A., 2017. Postglacial response of Arctic Ocean gas hydrates to climatic amelioration. Proc Natl Acad Sci U S A 114, 6215–6220. https://doi.org/10.1073/pnas.1619288114

Shipley, T.H., Houston, M.H., Buffler, R.T., Shaub, F.J., McMillen, K.J., Ladd, J.W., Worzel, J.L., 1979. Seismic Evidence for Widespread Possible Gas Hydrate Horizons on Continental Slopes and Rises. Am Assoc Pet Geol Bull 63, 2204–2213. https://doi.org/10.1306/2F91890A-16CE-11D7-8645000102C1865D

Skogseid, J., Eldholm, O., 1995. Rifted Continental Margin off Mid-Norway, in: Rifted Ocean-Continent Boundaries. pp. 147–153. https://doi.org/10.1007/978-94-011-0043-4_8

Sloan, E.D., Koh, C., 2007. Clathrate Hydrates of Natural Gases, Third Edition, Chemical Industries. CRC Press.

Solheim, A., Elverhøi, A., 1985. A pockmark field in the Central Barents Sea; gas from a petrogenic source? Polar Res 3, 11–19. https://doi.org/10.1111/j.1751-8369.1985.tb00492.x

Tamaki, M., Fujii, T., Suzuki, K., 2017. Characterization and Prediction of the Gas Hydrate Reservoir at the Second Offshore Gas Production Test Site in the Eastern Nankai Trough, Japan. Energies (Basel) 10, 1678. https://doi.org/10.3390/en10101678

Tishchenko, P., Hensen, C., Wallmann, K., Wong, C.S., 2005. Calculation of the stability and solubility of methane hydrate in seawater. Chem Geol 219, 37–52. https://doi.org/10.1016/j.chemgeo.2005.02.008

Tsuji, Y., Fujii, T., Hayashi, M., Kitamura, R., Nakamizu, M., Ohbi, K., Saeki, T., Yamamoto, K., Namikawa, T., Inamori, T., Oikawa, N., Shimizu, S., Kawasaki, M., Nagakubo, S., Matsushima, J., Ochiai, K., Okui, T., 2009. Methane-hydrate Occurrence and Distribution in the Eastern Nankai Trough, Japan: Findings of the Tokai-oki to Kumano-nada Methane-hydrate Drilling Program. Natural Gas Hydrates - Energy Resource Potential and Associated Geologic Hazards: AAPG Memoir 89 228–246. https://doi.org/10.1306/13201103M893129

Vadakkepuliyambatta, S., Bünz, S., Mienert, J., Chand, S., 2013. Distribution of subsurface fluid-flow systems in the SW Barents Sea. Mar Pet Geol 43, 208–221. https://doi.org/10.1016/j.marpetgeo.2013.02.007

Vadakkepuliyambatta, S., Chand, S., Bünz, S., 2017. The history and future trends of ocean warming-induced gas hydrate dissociation in the SW Barents Sea. Geophys Res Lett 44, 835–844. https://doi.org/10.1002/2016GL071841

Vogt, P.R., Cherkashev, G., Ginsburg, G., Ivanov, G., Milkov, A., Crane, K., Lein, A., Sundvor, E., Pimenov, N., Egorov, A., 1997. Haakon mosby mud volcano provides unusual example of venting. Eos (Washington DC) 78, 549–557. https://doi.org/10.1029/97eo00326

Vorren, T.O., Lebesbye, E., Andreassen, K., Larsen, K.B., 1989. Glacigenic sediments on a passive continental margin as exemplified by the Barents Sea. Mar Geol 85, 251–272. https://doi.org/10.1016/0025-3227(89)90156-4

Vorren, T.O., Richardsen, G., Knutsen, S.M., Henriksen, E., 1991. Cenozoic erosion and sedimentation in the western Barents Sea. Mar Pet Geol 8, 317–340. https://doi.org/10.1016/0264-8172(91)90086-G

Waage, M., Portnov, A., Serov, P., Bünz, S., Waghorn, K.A., Vadakkepuliyambatta, S., Mienert, J., Andreassen, K., 2019. Geological Controls on Fluid Flow and Gas Hydrate Pingo Development on the Barents Sea Margin. Geochemistry, Geophysics, Geosystems 20, 630–650. https://doi.org/10.1029/2018GC007930

Wei, L., Cook, A., Daigle, H., Malinverno, A., Nole, M., You, K., 2019. Factors Controlling Short-Range Methane Migration of Gas Hydrate Accumulations in Thin Coarse-Grained Layers. Geochemistry, Geophysics, Geosystems 20, 3985–4000. https://doi.org/10.1029/2019GC008405

Westbrook, G.K., Chand, S., Rossi, G., Long, C., Bünz, S., Camerlenghi, A., Carcione, J.M., Dean, S., Foucher, J.P., Flueh, E., Gei, D., Haacke, R.R., Madrussani, G., Mienert, J., Minshull, T.A., Nouzé, H., Peacock, S., Reston, T.J., Vanneste, M., Zillmer, M., 2008. Estimation of gas hydrate concentration from multi-component seismic data at sites on the continental margins of NW Svalbard and the Storegga region of Norway. Mar Pet Geol 25, 744–758. https://doi.org/10.1016/j.marpetgeo.2008.02.003

You, K., Flemings, P.B., Malinverno, A., Collett, T.S., Darnell, K., 2019. Mechanisms of Methane Hydrate Formation in Geological Systems. Reviews of Geophysics 57, 1146–1196. https://doi.org/10.1029/2018RG000638

Yun, T.S., Francisca, F.M., Santamarina, J.C., Ruppel, C., 2005. Compressional and shear wave velocities in uncemented sediment containing gas hydrate. Geophys Res Lett. https://doi.org/10.1029/2005GL022607